

LA-UR-06-4593

Approved for public release;
distribution is unlimited.

Title: Flux-based advection
vs.
the Lagrangian remap

Author(s): Vadim Dyadechko vdyadechko@lanl.gov
Mathematical Modeling and Analysis Group, T-7
Los Alamos National Laboratory

Submitted to: <http://math.lanl.gov/~vdyadechko/doc/2006-fluxing-vs-remap.pdf>



Los Alamos National Laboratory, an affirmative action/equal opportunity employer, is operated by the University of California for the U.S. Department of Energy under contract W-7405-ENG-36. By acceptance of this article, the publisher recognizes that the U.S. Government retains a nonexclusive, royalty-free license to publish or reproduce the published form of this contribution, or to allow others to do so, for U.S. Government purposes. Los Alamos National Laboratory requests that the publisher identify this article as work performed under the auspices of the U.S. Department of Energy. Los Alamos National Laboratory strongly supports academic freedom and a researcher's right to publish; as an institution, however, the Laboratory does not endorse the viewpoint of a publication or guarantee its technical correctness.

Flux-based advection vs. the Lagrangian remap

Vadim Dyadechko*

Draft of July 17, 2006; the first draft is dated April 28, 2006.

1 Motivation

Volume-of-Fluid (VoF) methodology for decades provided a robust material interfaces model for multi-material Eulerian/Arbitrary Lagrangian-Eulerian (ALE) fluid flow simulations. Instead of direct interface tracking, VoF methods calculate the interface location at each discrete moment of time from the solution data, namely from the volumes of the cell fractions occupied by different materials (phases). This strategy faces no problem changing the topology of the interface dynamically; the choice of the volume fractions as an input for the interface reconstruction allows to design the latter to be mass-conservative.

But the interface reconstruction algorithm is just one of the two constitutive parts of the typical VoF method. Another essential component of VoF method is an advection scheme, i.e. an algorithm to update the content of the cells at each time step. The cell content is traditionally updated by calculating of the material fluxes through the cell boundaries. This guarantees the conservation of the mass during the advection step and makes the whole VoF simulation cycle mass-conservative.

VoF methods are not free of drawbacks. The resolution of a generic VoF interface reconstruction algorithm is limited by the resolution of the grid: a characteristic size of the interface features that can be captured with VoF method is about 2 to 3 cell sizes. The recent introduction of the Moment-of-Fluid (MoF) technique showed the significant improvement of the resolution over the traditional VoF methods. The key difference between VoF methods and the MoF method is that the latter reconstructs the interfaces in mixed cells using not only the volumes, but also the centroids of the cell fractions.

The extended input data set for the MoF interface reconstruction demands more sophisticated advection scheme, capable of updating not only the volumes but also

*Mathematical Modeling and Analysis Group (T-7) at the Los Alamos National Laboratory; e-mail: vdyadechko@lanl.gov

the centroids. The example Lagrangian remap scheme [2] proposed to be used with MoF reconstruction serves the purpose well, but it extensively uses polygon (polyhedron in 3D) intersection, which many developers may consider to be excessively expensive.

The purpose of this paper is to describe a feasible flux-based advection scheme for 2D simulations capable of updating the first moment data and give an unbiased comparison of the flux-based advection scheme against the Lagrangian remap. We are not going to discuss the performance issues but mostly concentrate on the accuracy.

2 Flux-based advection scheme

(jointly with Rob Lowrie (CCS-2) and Mikhail Shashkov (T-7))

Consider a convex polygonal cell Ω given by its vertices V_1, \dots, V_n , $n \geq 3$. This cell does not stand along, but is a part of the conformal polygonal grid; the symbol Ω_i is used to denote the cell adjacent to Ω through the i -th edge $V_i V_{i+1}$, ($V_{n+1} \equiv V_1$), $i = \overline{1, n}$ (Figure 1a). Let $\omega^k \subset \Omega$ and $\omega_i^k \subset \Omega_i$ represent the dark material loci inside the respective cells Ω and Ω_i , $i = \overline{1, n}$ at $t = t^k = k\Delta t$, $k = 0, 1, 2, \dots$ (Figure 1b).

Both dark and light fluids are considered to be incompressible, therefore the velocity field $\mathbf{v}(\mathbf{x}, t)$ has to be solenoidal; for now let us assume that $\mathbf{v}(\mathbf{x}, t)$ is given analytically. It is convenient to consider a Lagrangian transformation \mathcal{L}^k that specifies the evolution of the geometrical set $\omega \subset \mathbb{R}^2$ in the given velocity field due to the k -th time step:

$$\mathcal{L}^k(\omega(t^{k-1})) = \omega(t^k).$$

The flux paradigm suggests to represent the change of the cell content as a result of the matter flow through the separate cell edges. This approach yields the following expressions for updating the zeroth and the first moments of the dark fluid inside the cell Ω on the k -th time step:

$$|\omega^k| = |\omega^{k-1}| + \sum_{i=1}^n (|\Delta^+ \omega_i^{k-1}| - |\Delta^- \omega_i^{k-1}|) \quad (1)$$

$$\mathbf{M}_1(\omega^k) = |\omega^{k-1}| \mathbf{x}_c(\mathcal{L}^k(\omega^{k-1})) + \sum_{i=1}^n (|\Delta^+ \omega_i^{k-1}| \mathbf{x}_c(\mathcal{L}^k(\Delta^+ \omega_i^{k-1})) - |\Delta^- \omega_i^{k-1}| \mathbf{x}_c(\mathcal{L}^k(\Delta^- \omega_i^{k-1}))) \quad (2)$$

These formulas require a bit of explanation. Here $\Delta^+ \omega_i$ and $\Delta^- \omega_i$ denote for the amounts of dark fluid that cross the the i -th edge of Ω between $t = t^{k-1}$ and $t = t^k$ in inward and outward directions respectively; $\Delta^+ \omega_i^{k-1}$ and $\Delta^- \omega_i^{k-1}$, particularly, specify the respective loci of these amounts at $t = t^{k-1}$.

Note that both (1) and (2) are exact. Let us look at how one can reasonably approximate $\Delta^+ \omega_i^{k-1}$ and $\Delta^- \omega_i^{k-1}$ to make these formulas work. The approximate update strategy may be the following:

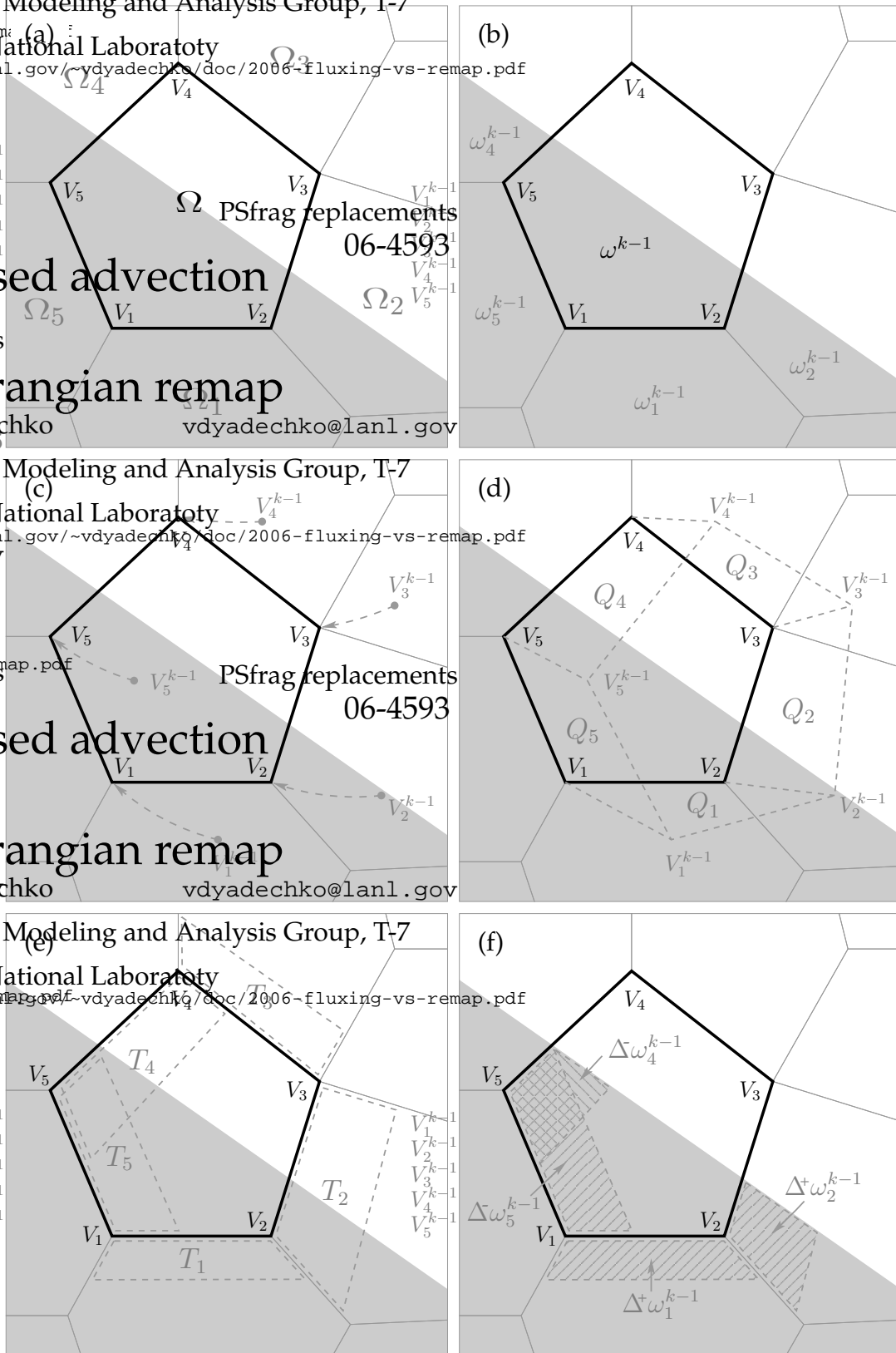


Figure 1. The flux-based advection scheme illustrated.

- 1) The ends of the edge are traced one step back in time (Figure 1c). Let V_i^{k-1} and V_{i+1}^{k-1} be the respective Lagrangian prototypes of V_i and V_{i+1} at $t = t^{k-1} = (k-1)\Delta t$. The algebraic (signed) area A_i of the quad $Q_i = V_i V_i^{k-1} V_{i+1}^{k-1} V_{i+1}$ (Figure 1d) is supposed to specify the amount fluid that moves through the edge $V_i V_{i+1}$.
- 2) If $A_i = 0$, then $\Delta^+ \omega_i^{k-1} = \Delta^- \omega_i^{k-1} = \emptyset$.
- 3) If the area A_i is positive, the fluid is considered to flow strictly inward, i.e. $\Delta^- \omega_i^{k-1} = \emptyset$. In this case the quad Q_i is replaced by the shortest trapezoid $T_i \subset \Omega_i$ of the equal area $|T_i| \equiv |A_i|$ with one of the bases given by the edge $V_i V_{i+1}$ (trapezoids T_4 and T_5 on Figure 1e). This substitution is possible only if $|\Omega_i| \leq |A_i|$, therefore the condition $CFL \leq 1$ is essential for this type of scheme. The intersection $T_i \cap \omega_i^{k-1}$ is going to represent $\Delta^+ \omega_i^{k-1}$ ($\Delta^+ \omega_4^{k-1}$ and $\Delta^+ \omega_5^{k-1}$ on Figure 1e).
- 4) If the area A_i is negative, the fluid is considered to flow strictly outward, i.e. $\Delta^+ \omega_i^{k-1} = \emptyset$. In this case the quad Q_i is replaced by the shortest trapezoid $T_i \subset \Omega$ of the equal area $|T_i| \equiv |A_i|$ with one of the bases given by the edge $V_i V_{i+1}$ (trapezoids T_1 , T_2 , and T_3 on Figure 1e). Once again, the substitution is possible only if $|\Omega| \leq |A_i|$, therefore the condition $CFL \leq 1$ is essential for this type of scheme. The intersection $T_i \cap \omega^{k-1}$ is going to represent $\Delta^- \omega_i^{k-1}$ ($\Delta^- \omega_1^{k-1}$ and $\Delta^- \omega_2^{k-1}$ on Figure 1e).
- 5) The centroid of $\mathcal{L}^k(\Delta \omega_i^{k-1})$ will be approximated as $\mathcal{L}^k(\mathbf{x}_c(\Delta \omega_i^{k-1}))$, i.e. by advecting the centroid of $\Delta \omega_i^{k-1}$ one time step forward as if it were a Lagrangian particle by means of the 4-th order Runge-Kutta method.
- 6) Similarly, the centroid of $\mathcal{L}^k(\omega^{k-1})$ will be approximated as $\mathcal{L}^k(\mathbf{x}_c(\omega^{k-1}))$, i.e. by advecting the centroid of ω^{k-1} one time step forward as if it were a Lagrangian particle by means of the 4-th order Runge-Kutta method.
- 7) Use equations (1) and (2) to update the volume and the first moment of the dark fluid enclosed in Ω .
- 8) Calculate the new centroid of the dark fluid as $\mathbf{x}_c(\omega^k) = M_1(\omega^k)/|\omega^k|$.
- 9) Due to the approximate nature of the volume update, it may happen that the new volume of the dark fluid is negative, or exceeds the volume of the cell. To eliminate these abnormalities, the global repair procedure (see [3] or [2]) has to be applied to the dark volumes after the update step. The lower \underline{m}^k and upper \overline{m}^k bounds of the new volume are selected as follows:
 - if $|\Omega| \leq |\omega^k|$ then

$$\underline{m}^k = \overline{m}^k = |\Omega|;$$
 - else if $|\omega^k| < 0$ then

$$\underline{m}^k = \overline{m}^k = 0;$$

otherwise

$$\underline{m}^k = 0 \text{ and } \overline{m}^k = |\Omega|.$$

The repair step concludes the description of the flux-based advection scheme.

3 Numerical tests

Let us compare the accuracies of the flux-based advection scheme and the original Lagrangian remap presented in [2]. We use the following technique to measure the accuracy of the scheme:

- 1) Let $\omega_{0,h}$ be the static reconstruction of the analytically given initial locus of the dark fluid ω_0 .
- 2) Move the fluid in a given static velocity field from $t = 0$ to $t = T/2$, then reverse the field and continue to move fluid until $t = T$. Let us denote the final locus of the dark fluid as $\omega_{T,h}$.
- 3) Use the area of the symmetric difference between $\omega_{0,h}$ and $\omega_{T,h}$ as the measure of the discrepancy of these two sets and the cumulative error of the interface tracking method:

$$\varepsilon = |\omega_{0,h} \Delta \omega_{T,h}|.$$

Every setup was tried with six different types of the interface tracking techniques: each of the two advection algorithms examined (fluxing and remap) was combined with each of the three interface reconstruction algorithms (VoF-LSGQ¹⁾ [1], VoF-Swartz [5, 4], and MoF [2]).

Each interface tracking technique was tested with four different mesh resolutions $h \in \{1/16, 1/32, 1/64, 1/128\}$ and seven different values of the Courant number $CFL \in \{1, 1/2, 1/4, 1/8, 1/16, 1/32, 1/64\}$. The time increment in each run is the function of h and CFL : $\Delta t = CFL h/v_{max}$, where v_{max} is the maximum velocity for the given velocity field. The total time $T = \Delta t/(CFL h) = 1/v_{max}$.

Test 1: diagonal translation.

The velocity field:

$$\mathbf{v}(\mathbf{x}) = (1/\sqrt{2}, 1/\sqrt{2})$$

with the maximum velocity $v_{max} = 1$.

The initial locus:

$$\omega_0 = \{ \mathbf{x} \in \mathbb{R}^2 \mid |\mathbf{x} - \mathbf{x}_0| \leq R_0 \}, \quad \mathbf{x}_0 = (0.25, 0.25), \quad R_0 = 0.15.$$

The corresponding error graphs are presented on Figures 2, 3, and 4.

Test 2: solid rotation.

¹⁾ For internal cells of the uniform rectangular grid LSGQ results in the same interface as the Youngs' algorithm with $\alpha = 2$.

The velocity field:

$$\mathbf{v}((x, y)) = \begin{bmatrix} -(y - y_0) \\ +(x - x_0) \end{bmatrix} / (2\pi R_{max}), \quad (x_0, y_0) = (0.5, 0.5), R_{max} = 0.5$$

with the maximum velocity $v_{max} = 1$ (assuming that $|(x, y) - (x_0, y_0)| \leq R_{max}$).

The initial locus:

$$\omega_0 = \{ \mathbf{x} \in \mathbb{R}^2 \mid |\mathbf{x} - \mathbf{x}_0| \leq R_0 \}, \quad \mathbf{x}_0 = (0.5, 0.75), R_0 = 0.15.$$

Note that the distance between any point of ω_0 and the rotation center (x_0, y_0) ranges from 0.1 to 0.4. The value of R_{max} has been deliberately set to exceed 0.4 to guarantee that no dark material will get out of the circle

$$\{ (x, y) \in \mathbb{R}^2 \mid |(x, y) - (x_0, y_0)| \leq R_{max} \}$$

and move faster than v_{max} , which is an essential requirement for the flux-based advection scheme.

The corresponding error graphs are presented on Figures 5, 6, and 7.

Test 3: vortex.

The velocity field:

$$\mathbf{v}((x, y)) = \begin{bmatrix} +\sin^2(\pi x) \sin(2\pi y) \\ -\sin^2(\pi y) \sin(2\pi x) \end{bmatrix}^T$$

with the maximum velocity: $v_{max} = 1$.

The initial locus is the same as for the solid rotation test:

$$\omega_0 = \{ \mathbf{x} \in \mathbb{R}^2 \mid |\mathbf{x} - \mathbf{x}_0| \leq R_0 \}, \quad \mathbf{x}_0 = (0.5, 0.75), R_0 = 0.15.$$

The corresponding error graphs are presented on Figures 8, 9, and 10.

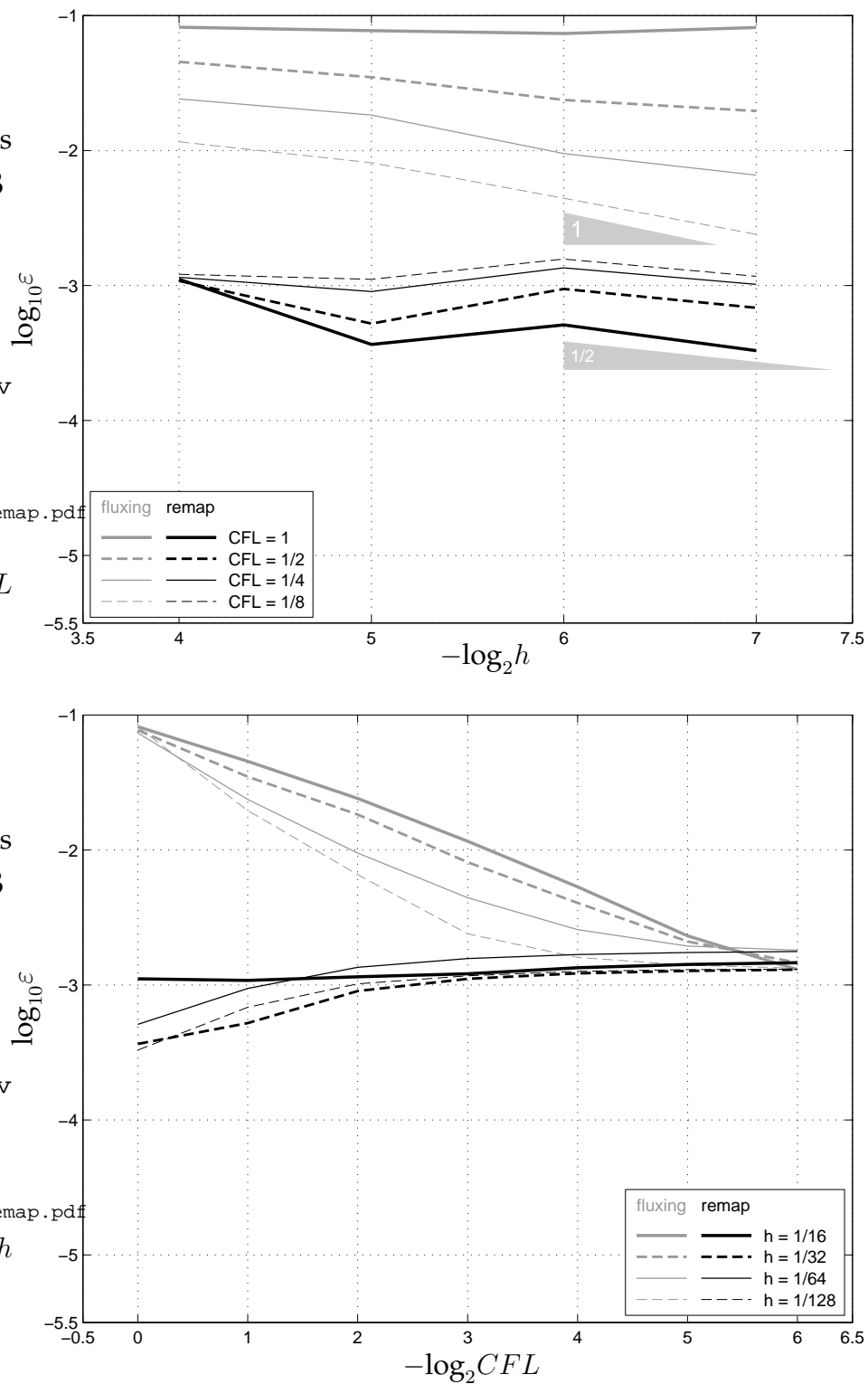


Figure 2. Two perspectives on the cumulative error ε measured in the **diagonal translation** tests with the **LSGQ** interface reconstruction.

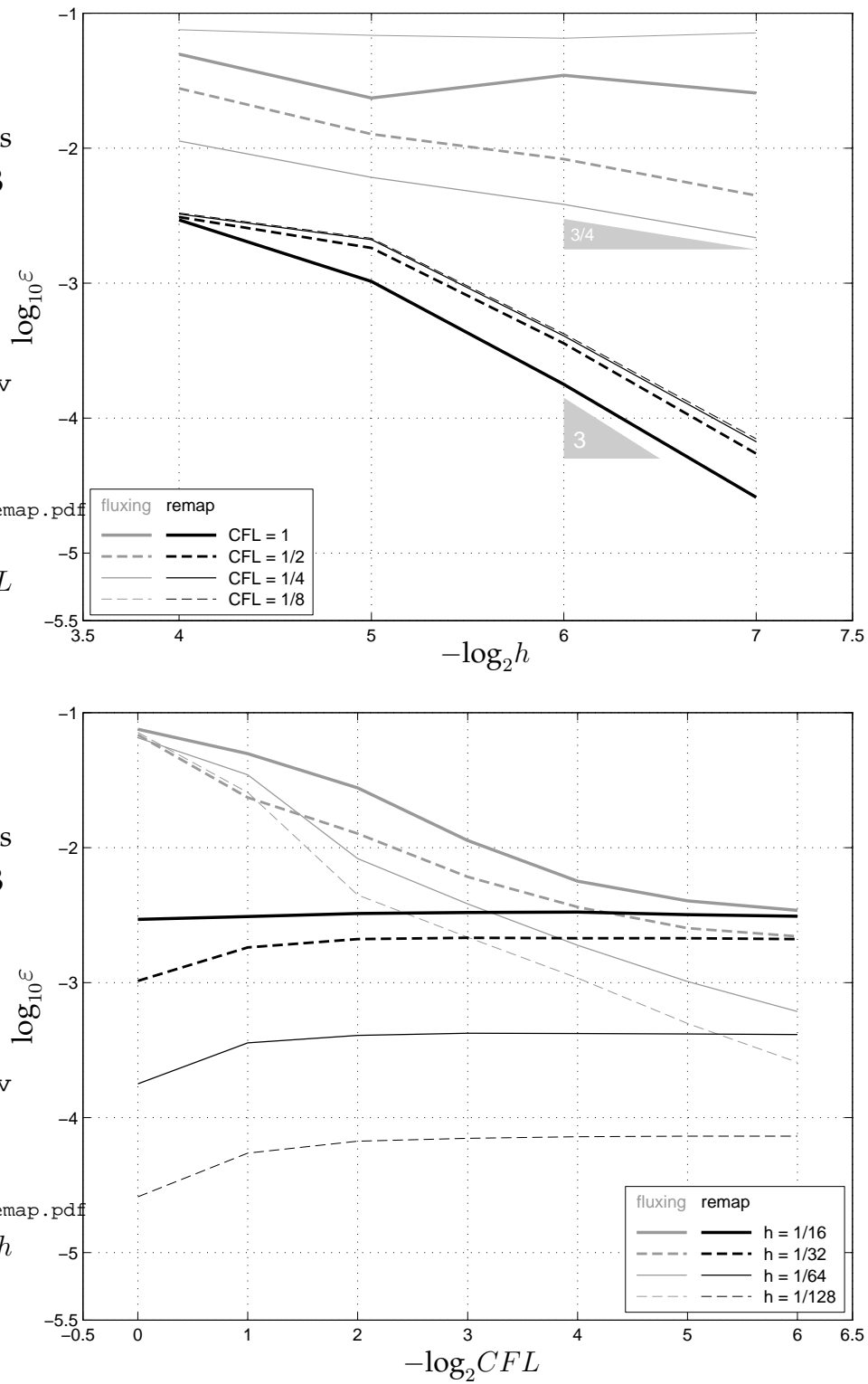


Figure 3. Two perspective on the cumulative error ε measured in the **diagonal translation test** with the **Swartz** interface reconstruction.

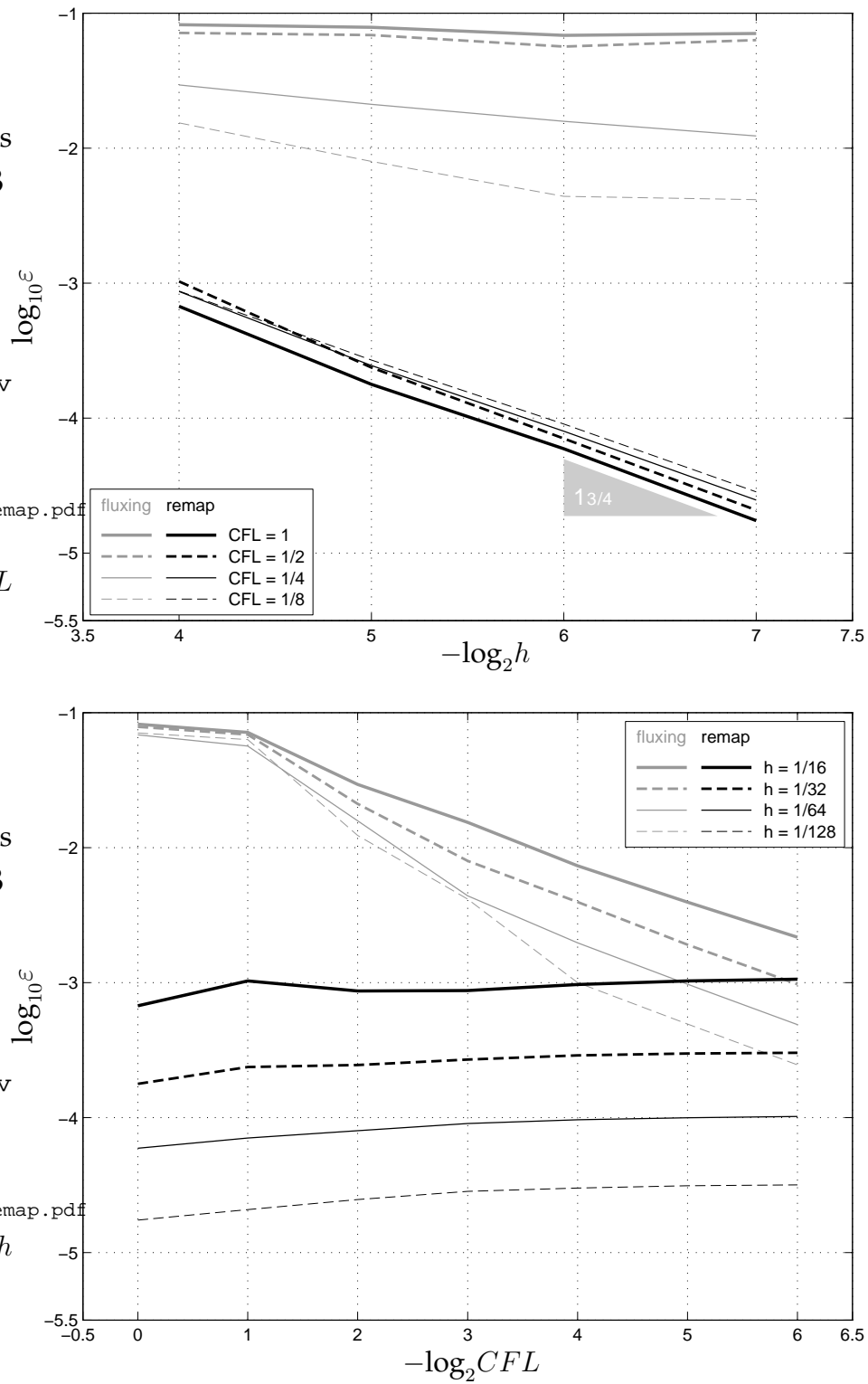


Figure 4. Two perspectives on the cumulative error ε measured in the **diagonal translation** tests with the **MoF** interface reconstruction.

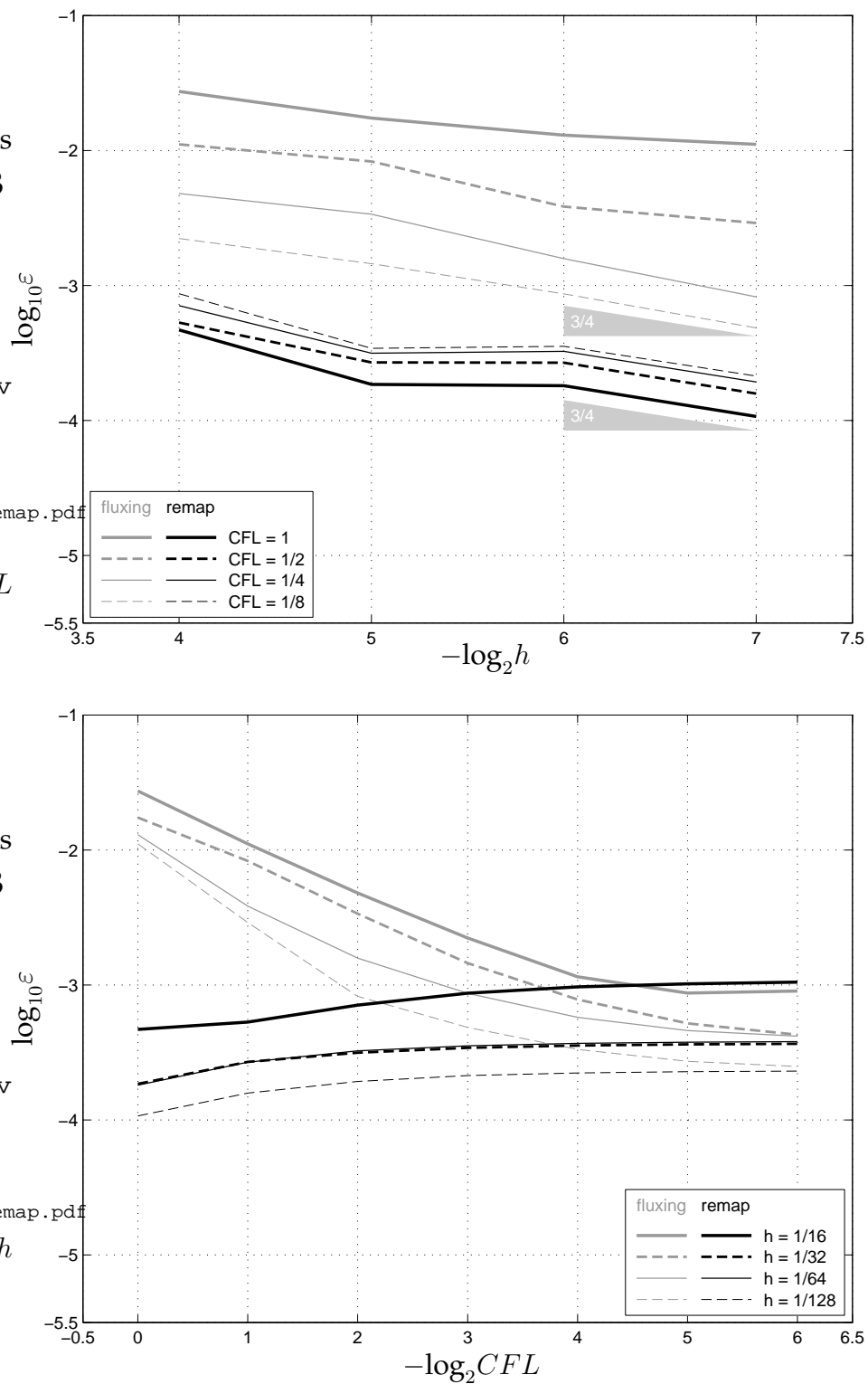


Figure 5. Two perspectives on the cumulative error ε measured in the **solid rotation** tests with the **LSGQ** interface reconstruction.

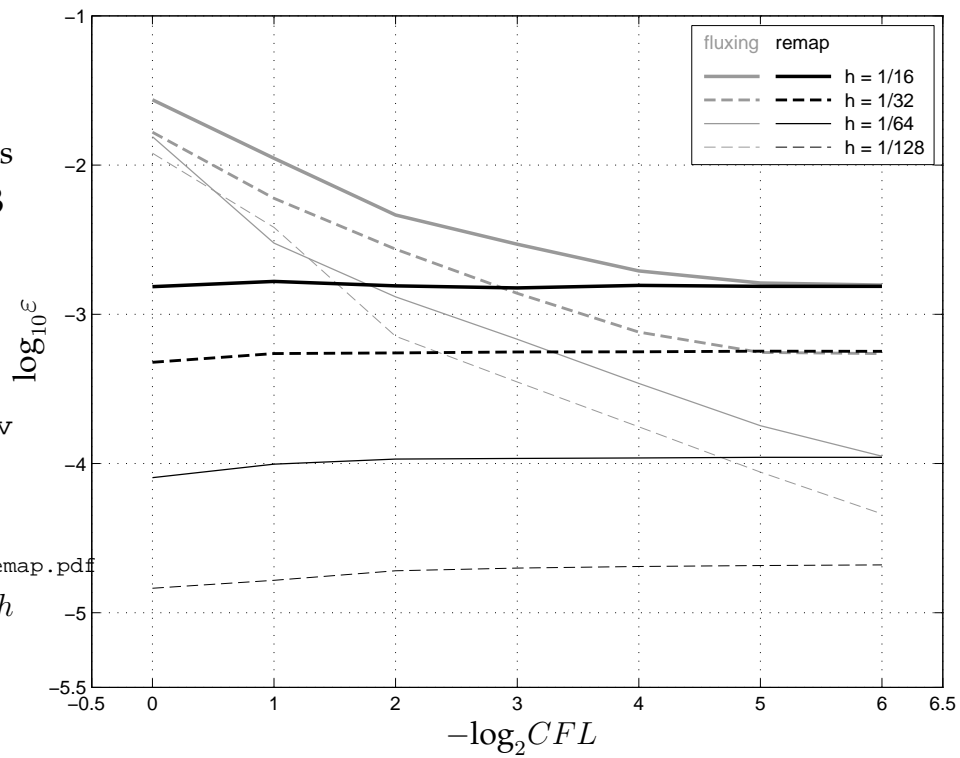
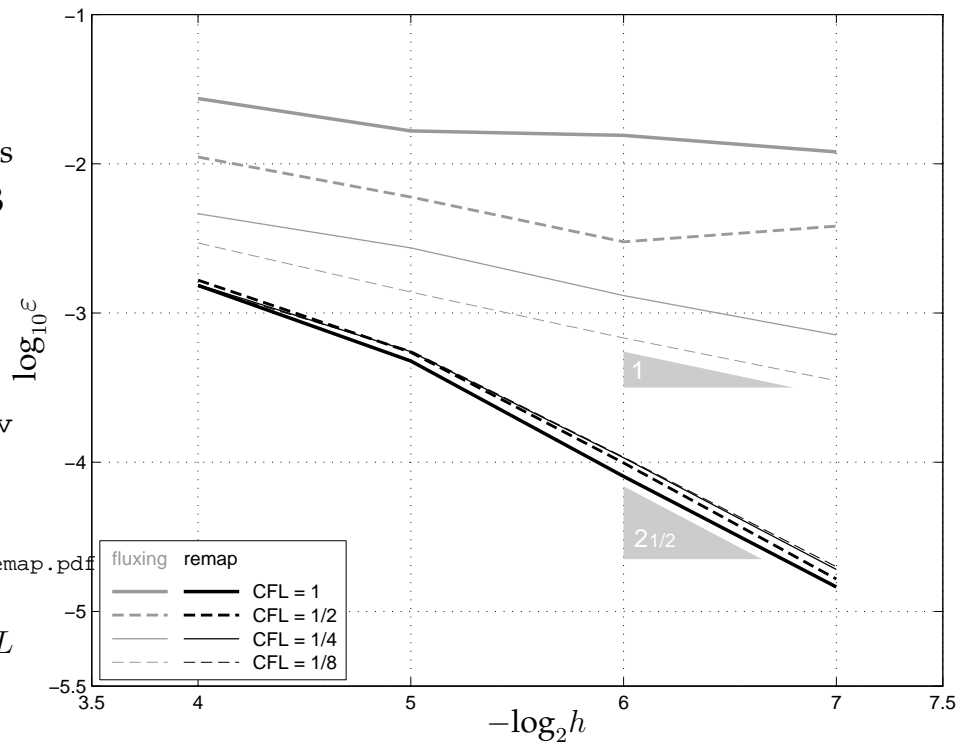


Figure 6. Two perspective on the cumulative error ε measured in the **solid rotation** test with the **Swartz** interface reconstruction.

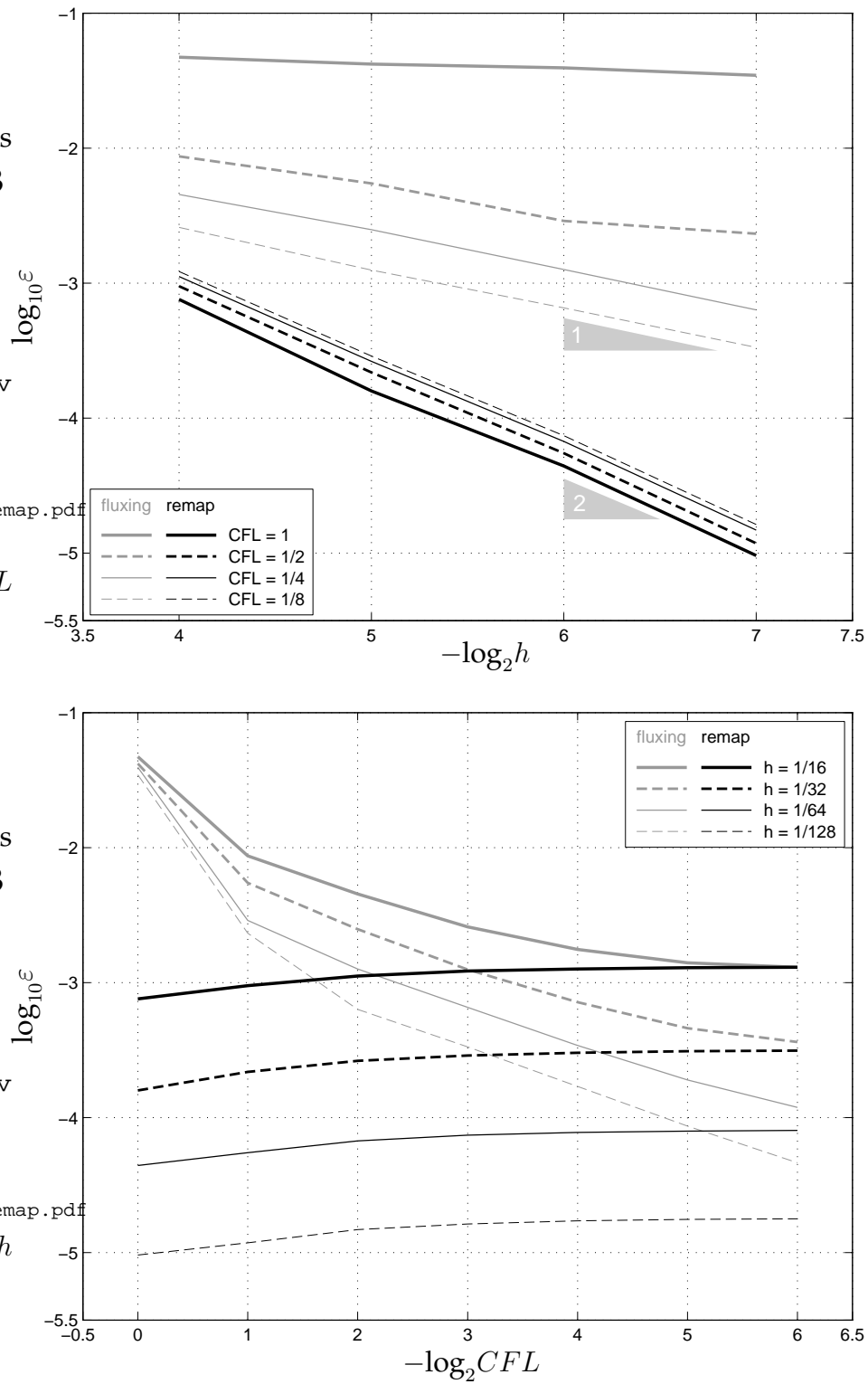


Figure 7. Two perspectives on the cumulative error ε measured in the **solid rotation** tests with the **MoF** interface reconstruction.

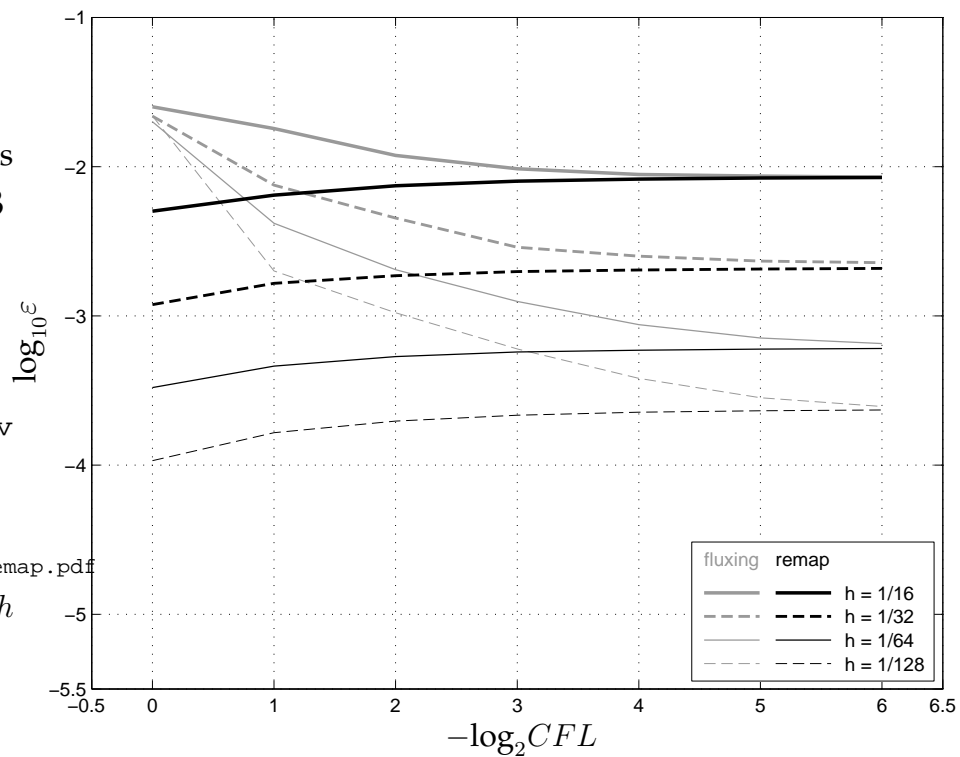
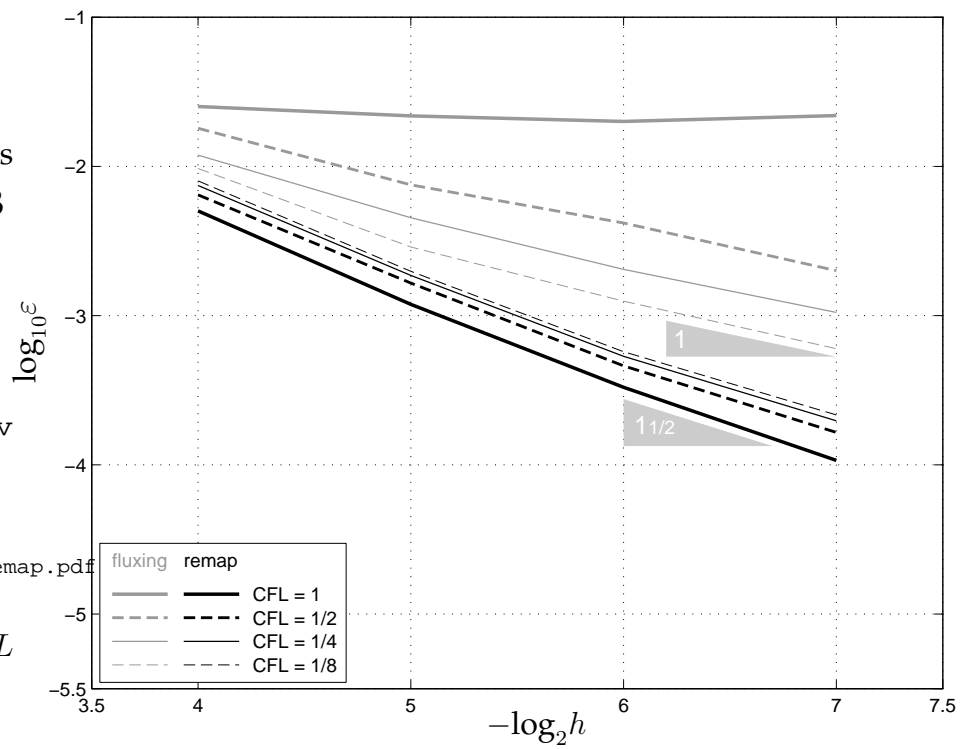


Figure 8. Two perspectives on the cumulative error ε measured in the **vortex** tests with the **LSGQ** interface reconstruction.

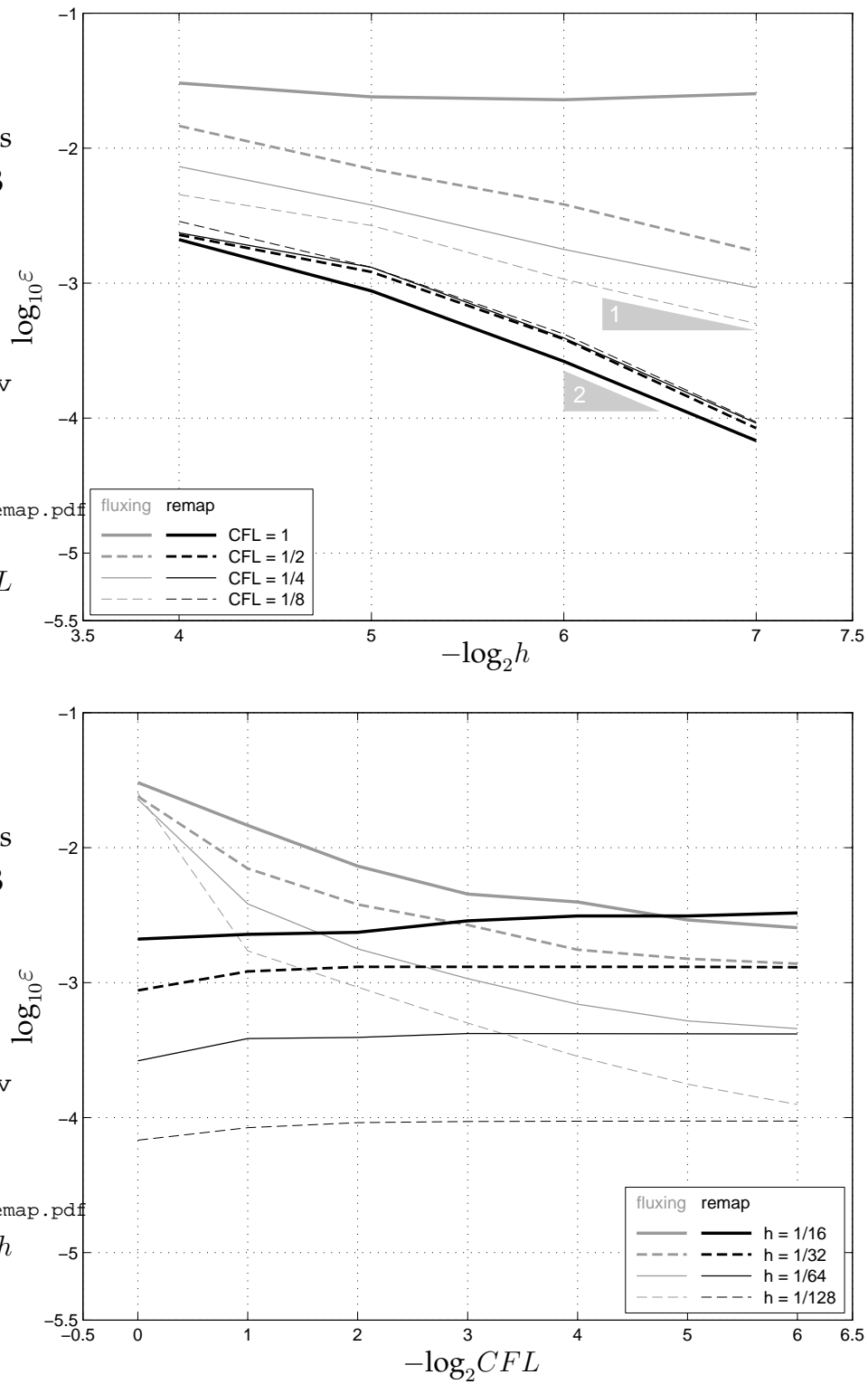


Figure 9. Two perspective on the cumulative error ε measured in the **vortex** test with the **Swartz** interface reconstruction.

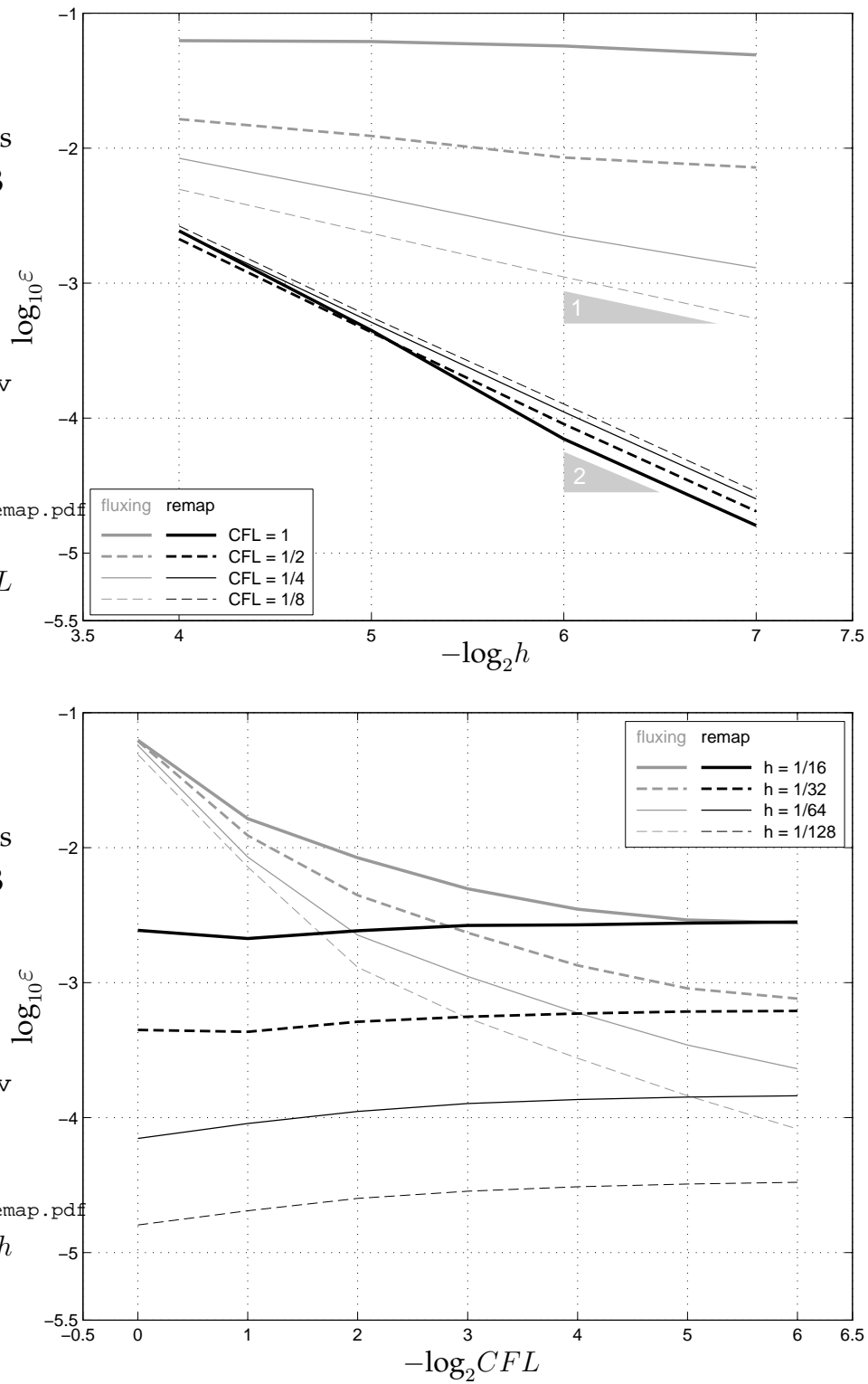


Figure 10. Two perspectives on the cumulative error ε measured in the vortex tests with the MoF interface reconstruction.

3.1 Summary of the numerical results

Although it is premature to discuss the performance issues (the implementations of both advection schemes are not optimal), it is worth noting that neither of the schemes showed a definitive advantage over the other.

As for the accuracy:

- 1) One can see that, with all other parameters being identical, the remapping is surely more accurate than the fluxing.
- 2) With reasonable discretization parameters ($h = 1/32$ and $CFL = 1/4$ in our case) the remap error is one to two orders of magnitude less than the fluxing error. As h becomes smaller, the supremacy of the remapping only gets more obvious.
- 3) The asymptotic ($h \rightarrow 0$) order of accuracy of the remapping scheme is on average one order higher than the asymptotic accuracy of the fluxing scheme.
- 4) The usage of the first order accurate interface reconstruction (LSGQ) significantly diminishes the overall accuracy. The error data may show sub-linear convergence or no convergence at all, which is not a surprise.
- 5) The remapping error shows no significant dependence on the Courant number: it grows very slowly, approaching a horizontal asymptote specific for the given grid resolution, as $CFL \rightarrow 0$. This behaviour can be explained by the growing frequency of the interface reconstruction invocations, all contributing to the final error.

The fluxing error, on the other hand, rapidly drops as CFL becomes smaller. But as $CFL \rightarrow 0$, the graph becomes asymptotically horizontal. Note that the fluxing-error floor is the same as the ceiling of the remapping error.

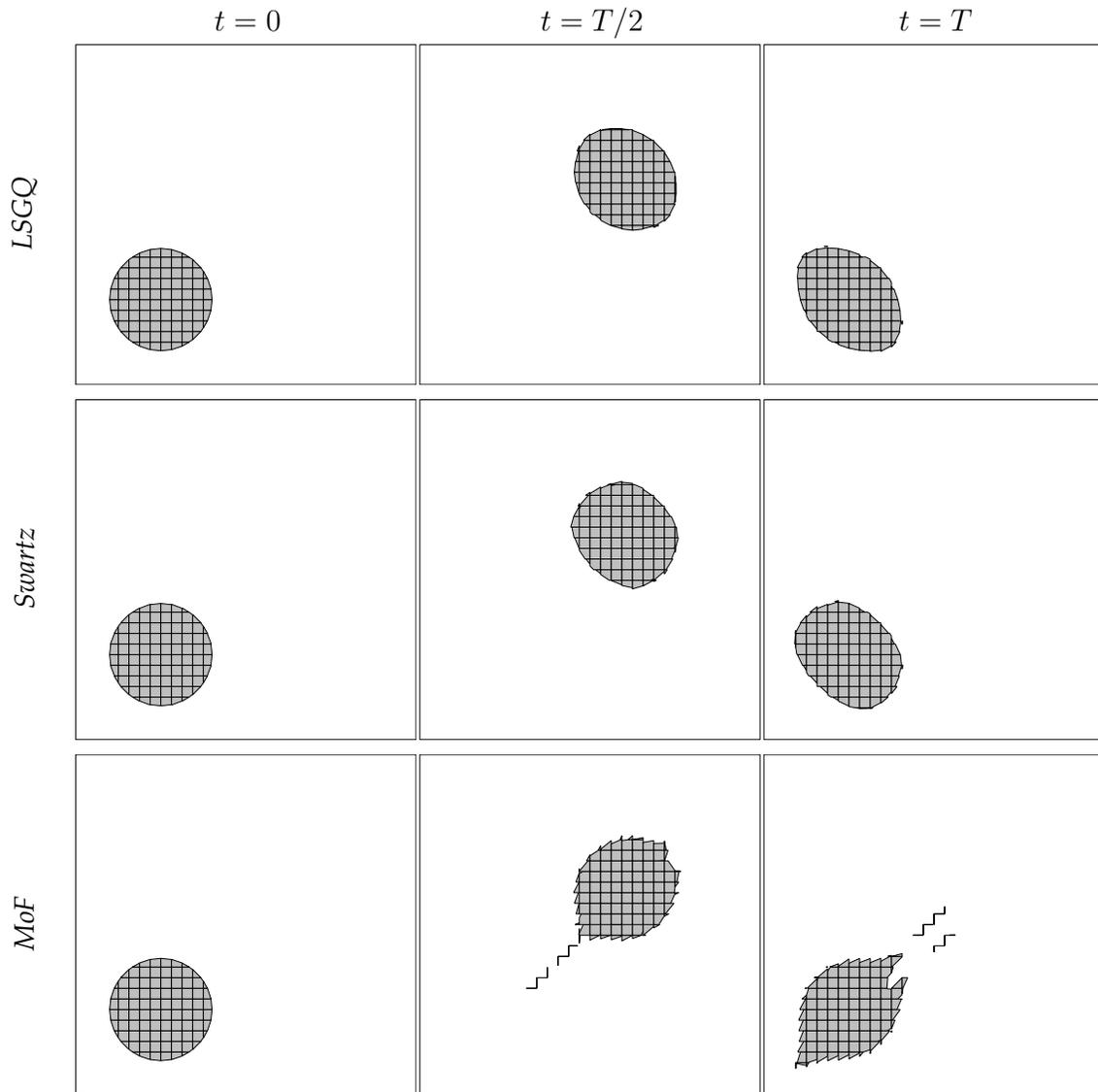


Figure 11. Snapshots: **diagonal translation** test with the **flux-based advection**;
 $h = 1/32$, $CFL = 1/4$.

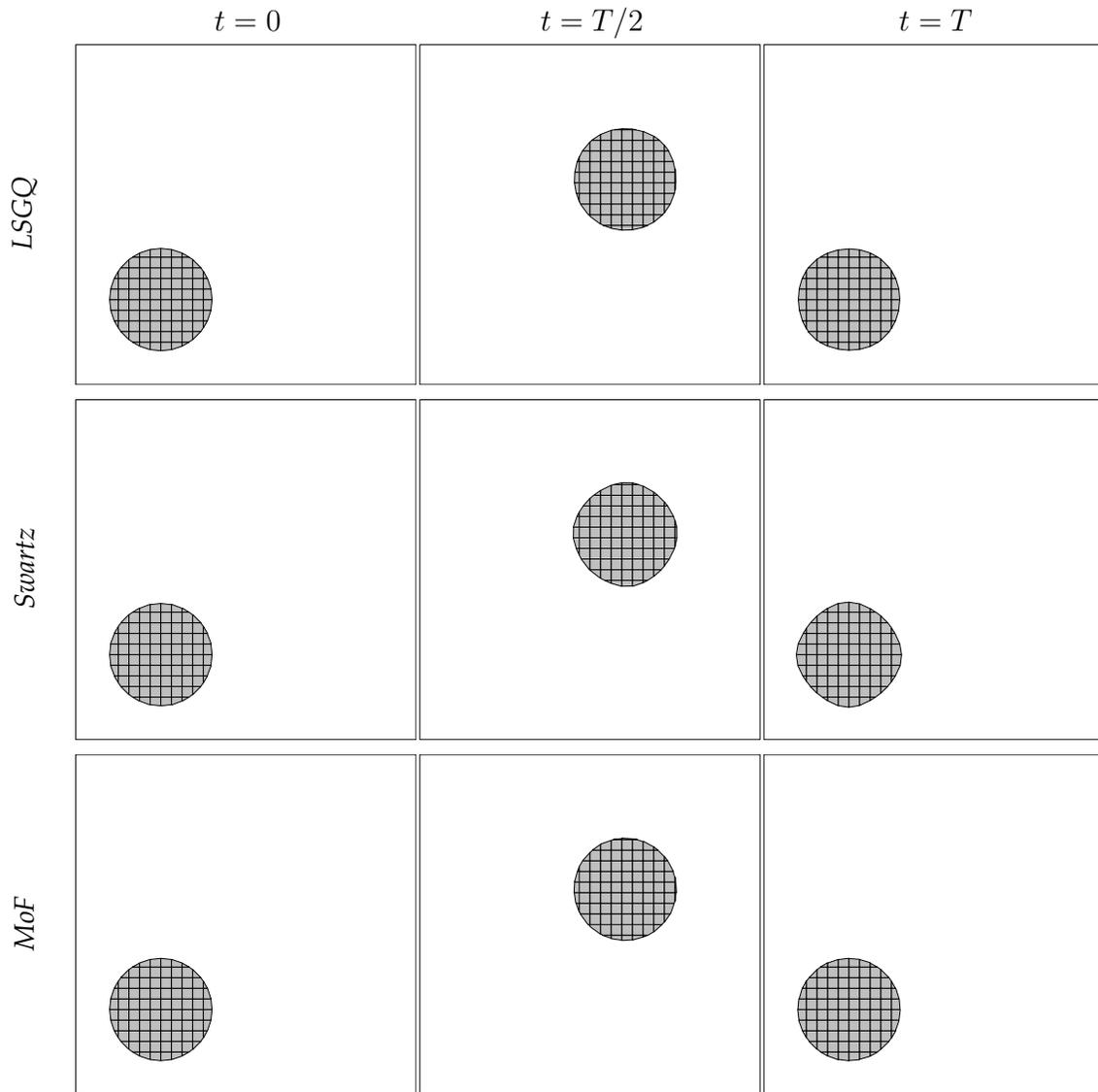


Figure 12. Snapshots: **diagonal translation** test with the **Lagrangian remap advection**; $h = 1/32$, $CFL = 1/4$.

References

- [1] Timothy J. Barth. Numerical methods for gasdynamic systems on unstructured meshes. In D. Kröner, M Ohlberger, and C. Rohde, editors, *An Introduction to Recent Developments in Theory and Numerics for Conservation Laws. Proceedings of the International School on Theory and Numerics for Conservation Laws, Freiburg/Littenweiler, October 20–24, 1997*, Lecture Notes in Computational Science and Engineering, pages 271–273. Springer-Verlag, Berlin Heidelberg, 1999.
- [2] Vadim Dyadechko and Mikhail Shashkov. Moment-of-fluid interface reconstruction. Technical Report LA-UR-05-7571, Los Alamos National Laboratory, Los Alamos, NM, Oct 2005.
- [3] R. V. Garimella, V. Dyadechko, B. K. Swartz, and M. Shashkov. Interface reconstruction in multi-fluid, multi-phase flow simulations. In *Proceedings of the 14th International Meshing Roundtable*, pages 19–23, San Diego, CA, 2005.
- [4] S. J. Mosso, B. K. Swartz, D. B. Kothe, and R. C. Ferrell. A parallel, volume-tracking algorithm for unstructured meshes. In P. Schiano, A. Ecer, J. Periaux, and N. Satofuka, editors, *Parallel Computational Fluid Dynamics: Algorithms and Results Using Advanced Computers*, pages 368–375. Elsevier Science, 1997.
- [5] Blair Swartz. The second-order sharpening of blurred smooth borders. *Mathematics of Computation*, 52(186):675–714, Apr 1989.